From waste to waste treatment: Mesoporous magnetic NiFe2O4/ZnCuCr-layered double hydroxide composite for wastewater treatment

Zhang, Rose; Xia, Bangwang; Wang, Peipei; Wang, Yi; Li, Zhidao; Wang, Youchen; Feng, Lei; Li, Xiaona; Du, Shangfeng

DOI:
10.1016/j.jallcom.2019.153053

Document Version
Early version, also known as pre-print

Citation for published version (Harvard):
Zhang, R, Xia, B, Wang, P, Wang, Y, Li, Z, Wang, Y, Feng, L, Li, X & Du, S 2019, 'From waste to waste treatment: Mesoporous magnetic NiFe2O4/ZnCuCr-layered double hydroxide composite for wastewater treatment', *Journal of Alloys and Compounds*, vol. 819, 153053. https://doi.org/10.1016/j.jallcom.2019.153053

From Waste to Waste Treatment: Mesoporous Magnetic $NiFe_2O_4$/ZnCuCr-Layered Double Hydroxide Composite for Wastewater Treatment

Huixin Zhang[a*], Peipei Wang[a], , Xiuhong Jin[b], Bangwang Xia[a] Zhidao Li[a], Youchen Wang[a]

[a] School of Chemistry and Chemical Engineer, Hebei Univeristry of Technology, Tianjin 300130, China

[b] CNOOC Tianjin Chemical Research and Design Institute, Tianjin, 300131, China

Abstract:

Mesoporous magnetic $NiFe_2O_4$/ZnCuCr-LDH composite is synthesized by an environmental-friendly hydrothermal process from saccharin wastewater to achieve the goal of "treating the wastes with wastes". During this process, all waste iron-catalyst and 82% of COD are removed from the wastewater. The composite is characterized by FT-IR, XRD, SEM, XPS, BET and VSM analyses and its potential for wastewater treatment is evaluated by Congo Red (CR) adsorption. An over 97% removal efficiency is achieved with an initial CR concentration ranging from 100 ~ 450 mg/L. The adsorption kinetic is investigated and it is found that the experimental data agrees well with the pseudo-second-order kinetic model, intra-particle diffusion and Langmuir adsorption isotherm model. Adsorption isotherm indicates a spontaneous and endothermic adsorption type. The adsorption mechanism is also explored and the important roles of electrostatic attraction and anion exchange are demonstrated.

Key words: Wastewater; $NiFe_2O_4$; LDH; Adsorption; Congo red

1. Introduction

Industrial effluents such as saccharin wastewater, electroplating wastewater, heavy metal wastewater discharged into the environment has become a global concern due to freshwater crisis[2]. Saccharin wastewater is one of the wastewater that are the most difficult to be disposed. Saccharin is featured with its complex composition, high colority, high CODcr, high BOD_5, high salinity and low pH [3]. Among all dyes in saccharin wastewater, more than 70% are azo compounds which contain one or more azo bonds as the chromophore group[4; 5] designed to be resistant to light, weather, water, detergent and biodegradation in aerobic conditions and are remarkably steady. Therefore, it is necessary to be treated ahead of its discharge to the environment. To remove heavy metal ions and impurities, various treatment techniques[6] such as adsorption[7], chemical precipitation, ion exchange[8], membrane filtration[9; 10], coagulation[11], photocatalysis[12] and biological oxidation[13] have been investigated. So far, adsorption is accepted as an effective and environment-friendly method for

heavy metal wastewater treatment. Many traditional adsorbents such as activated carbon[14], clay[15], silicon nanomaterial[16], and metal oxides[17] have been studied. However, it's still a challenge to develop adsorbents with a low cost, high recyclability and easy separation ability.

Recently, magnetic nanoparticles such as magnetite (Fe_3O_4), maghemite (γ-Fe_2O_3) and spinel ferrite have attracted considerable attention in wastewater treatment due to their high surface-to-volume and magnetic properties[18]. In particular, heavy metal ions in wastewater can be employed as the raw materials to synthesize spinel ferrite. Chen et al.[19] reported that heavy metals from electroplating wastewater (EPW) and pickling waste liquor (PWL) fix into stable components of ferrite lattice. Among various spinel ferrite, $NiFe_2O_4$ nanoparticles are particularly attractive because of their high saturation magnetization, easy separation ability and good performance in scavenging hazardous pollutants [20].

Another method in the synthesis of solid phase to simultaneously scavenging the ions in wastewater is the preparation of layered double hydroxides [LDHs][2]. LDHs with their high surface area, high porosity and good anion exchange property have exerted some promising applications in adsorption. Pollutant anions can be scavenged in the synthesis of LDHs, because anions could intercalate between the layers[26]. Furthermore, the photo-decomposition of organic compounds is facilitated with LDHs composing of various metals such as Zn, Ni, and Cr. The hydrothermal method and co-precipitation[28] are the popular methods used for the preparation of LDHs, but when organic guest species with a low affinity to LDHs are intercalated into the interlayers, the ion exchange and co-precipitation methods are not applicable any more, the hydrothermal method is usually used. This method has been shown to be highly effective, because only the desired organic anions can occupy the interlayer space in LDHs under the hydrothermal condition in addition to the insoluble magnesium and aluminium hydroxides resourced from their precursors. Lei et al.[29] have demonstrated that Ni/Mg/Al LDH prepared by hydrothermal method exhibited excellent adsorption performances.

Therefore, a high potential is expected for the adsorption in wastewater treatment if we can combine the easy separation ability of ferrites and the high adsorbability of LDHs to develop magnetic composites[30] to control both the material microstructure and their macro-appearance in the co-existence of various complex components in wastewater. Herein, in this work, we investigate a facile process to prepare $NiFe_2O_4$/ZnCuCr-LDH composites via the hydrothermal method from saccharin wastewater to achieve the goal of "treating the wastes with wastes". The wastewater treatment potential is studied by using a simulated Congo Red (CR) adsorption with different contact times, adsorbent dosages, pHs and CR initial concentrations. The experimental adsorption data is also compared with various models to explore the adsorption mechanism.

2. Experimental section

2.1 Materials

Saccharin wastewater was provided by a local saccharin manufacturer in Tianjin in

China, containing 44.8 g Fe/L. The chemicals in analytical grade including $NiSO_4$, $Cu(NO_3)_2$, $Zn(NO_3)_2$, $Cr(NO_3)_3$, NaOH and $NaClO_3$?? were purchased from Tianjin Fuchen Chemical Reagent Co., Ltd. Congo red ($C_{28}H_{31}ClN_2O_3$) was provided by Tianjin Fengchuan Chemical Technology Co. Ltd. 1 g/L CR solution was prepared by dissolving 1.0000 g CR in 1 L deionized water, and other concentrations of CR was obtained by diluting.

2.2 Methods

2.2.1 Synthesis of $NiFe_2O_4$ nanoparticles

0.012 mol $NaClO_3$ was added into 25 ml saccharin wastewater to oxidize Fe^{2+} into Fe^{3+}(0.02 mol) followed by 0.01 mol $NiSO_4$. The pH value was adjusted to 9.0 by adding NaOH under vigorous stirring for 30min. After then, the above alkali solution was transferred into a 100 mL Telfon lined stainless steel autoclave. The autoclave was sealed and heated at 150 °C for 12 hours, then cooled down to room temperature in air. The obtained $NiFe_2O_4$ product was filtered and washed with deionized water and absolute ethanol several times, and dried at 60 °C overnight.

2.2.2 Synthesis of $NiFe_2O_4$/ZnCuCr-LDH composite

The molar ratio of Zn^{2+}, Cr^{3+} and Cu^{2+} was 2:1:9. All the chemicals were dissolved in 25 mL of deionized water. NaOH solution was used to adjust the pH to 5.5 under vigorous stirring. Then the obtained $NiFe_2O_4$ powder was dispersed into the above solution at a molar ratio of $NiFe_2O_4$/LDH of 0.3 and ultrasonically treated for 15 minutes at room temperature in air. After then, the suspension was transfered into the stainless steel autoclave with Teflon liner. The hydrothermal treatment was conducted at 150 °C for 12 hours. Subsequently, the as-prepared $NiFe_2O_4$/ZnCuCr-LDH composite was dried at 60 °C overnight. In comparison, pure ZnCuCr-LDH was also prepared in the similar way without $NiFe_2O_4$ addition as the bench sample.

2.3 Adsorption tests

The wastewater treatment performance of the $NiFe_2O_4$/ZnCuCr-LDH was evaluated by the CR adsorption on a water bath thermostatic oscillator at a constant shaking speed of 130 rpm in conical flasks. Adsorption procedure for single-factor experiments was performed by varying the contact time (0 ~ 720 min), adsorbent dosage (5 ~ 17.5 g/L), initial pH value (2 ~ 9) and initial CR concentration (100 ~ 450 mg/L). The initial pH of the dye solution was adjusted by 0.1 mol/L nitric acid and 0.1 mol/L sodium hydroxide. The solution volume in conical flask was 20 mL and the temperature of each experiment was 298 K. After adsorption, the residual CR was determined by a UV-vis spectrophotometer at 497.2 nm after the separation of adsorbent by a magnet. The removal efficiency (R, %) and the amount of CR adsorbed per unit mass of the adsorbents (q, mg/g) were evaluated from Eq. (1) and Eq. (2).

$$R = \frac{C_0 - C_e}{C_0} \times 100\% \quad (1)$$

$$q_t = \frac{(C_0 - C_e)V}{m} \times 100\% \quad (2)$$

where C_0 and C_t (mg/L) are the concentrations of CR in the solution at the initial time and final time, respectively; V (mL) is the initial volume of the CR solution, and m (g) is the mass of the adsorbent.

The same experimental process was conducted to the kinetic and isotherm experiments. In the adsorption kinetics, the aqueous samples were taken at desired time points (5, 10, 15, 20, 25, 30, 40, 60, 120, 240 and 480 min). Adsorption isotherm was studied at different temperatures (293, 298, 303, 308 K). The residual concentrations of CR were measured using the same method as the above UV-vis analysis.

2.4 Characterizations

Powder X-ray diffraction (XRD) patterns of the $NiFe_2O_4$, ZnCuCr-LDH, $NiFe_2O_4$/ZnCuCr-LDH were recorded using a Bruker D8 Advanced XRD diffractometer at Cu Kα radiation (λ=0.15418 Å) at 40 kV and 40 mA with a scanning rate of 5° min^{-1} between 5 and 80°. The Fourier transfer infrared (FT-IR) spectra were recorded by a FT-IR spectrometer (TENSOR 27, Bruker, Germany) with KBr pellets in the range of 4000 - 400 cm^{-1}. A scanning electron microscope (SEM) (FEI Quanta 450 FEG FESEM) was used to study the surface morphology of $NiFe_2O_4$, ZnZrCr-LDH and $NiFe_2O_4$/ZnZrCr-LDHs. N_2 adsorption–desorption isotherms were measured by using a Micromeritics analyser (America ASAP 2420). The specific surface areas were evaluated using Brunauer–Emmett–Teller (BET) method based on the adsorption isotherm. X-ray photoelectron spectroscopy (XPS, Escalab 250Xi, Thermo Fisher Scientific) was utilized to evaluate the surface chemical structure of the ZnCuCr-LDH nanoparticles. The radiation source was Al Kα (at pressure of - mbar) and the shift of binding energies (BE) was calibrated with respect to the reference peak of carbon at binding energy of - eV. Magnetic curves were recorded by a Vibrating sample magnetometer (740, LAKESHORE, America). The (dye) concentrations were determined photometrically on UV-Vis spectrophotometer (Lambda 25, Perkin Elmer, America).

3. Results and Discussion

3.1 Characterizations

Fig. S4 shows the magnetization curves of $NiFe_2O_4$/ZnCuCr-LDH and pure $NiFe_2O_4$. The saturated magnetization(Ms) of pure $NiFe_2O_4$ is 35.48 emu/g and the composite containing 30% $NiFe_2O_4$ exhibits a ferromagnetic behavior with the values of Ms of 10.82 emu/g. As shown in the inset of Fig. S4, $NiFe_2O_4$/ZnCuCr-LDH can be separated quickly from the suspension solution with the volume concentration of 25g/L after being magnetized by an external magnet in 12 seconds. Magnetic separation is particularly fulfilling because it conquers many of the problems which present in filtration, centrifugation or gravitational separation of nano-materials. It

requires less energy to attain a satisfied separation, in addition, it enhances the reusability of metal resources recovered from the wastewater.

Fig. 1 shows the SEM images of pure ZnCuCr-LDH and $NiFe_2O_4$/ZnCuCr-LDH composite. The pure ZnCuCr-LDH are small platelets with a smooth surface and size of ca. 1 μm (Fig. 1a). After been prepared to the $NiFe_2O_4$/ZnCuCr-LDH composite (Fig. 1b), some particles can be clearly seen on the surface, indicating the successful adhesion of $NiFe_2O_4$ nanoparticles to the layer-like LDHs.

Fig.1. SEM images of ZnCuCr-LDH (a) and $NiFe_2O_4$/ZnCuCr-LDH (b)

To confirm the crystal structure of the as-prepared materials, the XRD patterns of the prepared ZnCuCr-LDH, $NiFe_2O_4$/ZnCuCr-LDH and $NiFe_2O_4$ are displayed in Fig. 2. The diffraction peaks of $NiFe_2O_4$ /ZnCuCr-LDH at 2θ = 10, 20, 33 and 59° can be assigned to (003), (006), (012) and (110) crystal facets of ZnCuCr-LDH[32], another set of diffraction signals approximately at 2θ = 30, 35, 43, 57 and 63° are assigned to (220), (311), (400), (440), (511) and (422) of single phase cubic spinel structure of $NiFe_2O_4$[33]. This demonstrates both $NiFe_2O_4$ and ZnCuCr-LDH phases in the composite. Furthermore, after the surface decoration with $NiFe_2O_4$ nanoparticles, the regularity of LDH will be decreased, which is also confirmed by the broaden peaks and the reduced intensity of (003) and (006) peaks. The interlayer space (d_{003}) of pure LDH increased from 0.887 to 0.897 nm for the $NiFe_2O_4$/ZnCuCr-LDH composite. The reason is that LDH layer board is influenced by $NiFe_2O_4$ magnetic materials. SEM and XRD analyses prove the successful synthesis of the $NiFe_2O_4$/ZnCuCr-LDH composite and the surface modification of ZnCuCr-LDH by $NiFe_2O_4$ nanoparticles.

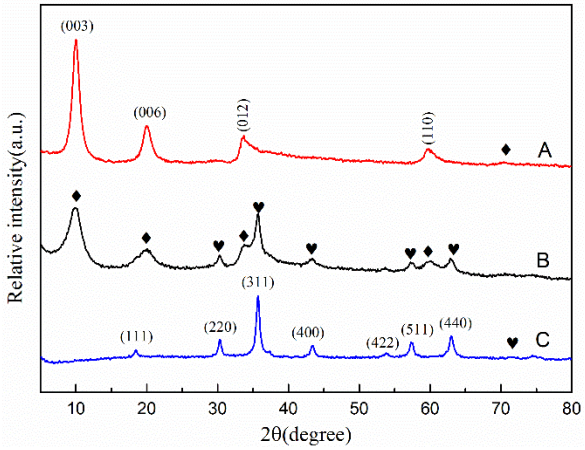

Fig. 2. XRD patterns of (A) ZnCuCr-LDH, (B) $NiFe_2O_4$/ZnCuCr-LDH, (C) $NiFe_2O_4$

To check the influence of the surface modification, the IR analysis of the $NiFe_2O_4$, $NiFe_2O_4$/ZnCuCr-LDH and ZnCuCr-LDH materials were conducted with KBr pellets in the range between 4000 - 400 cm^{-1} (Fig. S1). A strong and broad absorption band at 3417 cm^{-1} is indexed to the stretching vibrations of HOH and water molecules in the

interlayer space. The weak absorption band at 1625 cm^{-1} is resulted from the bending vibrations of OH. In particular, the absorption bands at 1384 cm^{-1} and 833 cm^{-1} are assigned to the vibrations of interlayer nitrate ion[31]. Besides, three adsorption bands below 700 cm^{-1} are attributed to the lattice vibration modes of the M−H vibration centered at about 600 cm^{-1} and the M−OH vibration at about 568 cm^{-1} and 507 cm^{-1} in the brucite-like layers. Compared to $NiFe_2O_4$ and LDH, the absorption bands around 571 cm^{-1}, 511 cm^{-1} and 625 cm^{-1} are red-shifted for the $NiFe_2O_4$/ZnCuCr-LDH composite. The is ascribed to the enhanced bond strength of the M-O-M formed from M-O in $NiFe_2O_4$ and M−OH in ZnCuCr-LDH.

Fig. S2 exhibits the XPS spectra of the $NiFe_2O_4$/ZnCuCr-LDH composite. The survey XPS spectra confirms the elements of Ni, Fe, O, Zn, Cu, Cr and C. Compared to the pure $NiFe_2O_4$ and the pure LDH, generate displacement is found to the peaks of every elements for $NiFe_2O_4$/ZnCuCr-LDH [34] and the comparision are showed in Fig. S3b, c, d, e, f, g. This shift results from the electronic coupling effect between $NiFe_2O_4$ and LDH which finally accelerates the electron-hole separation process.

A nitrogen adsorption-desorption measurement was conducted to characterize the specific surface area and internal pore superstructure of the $NiFe_2O_4$/ZnCuCr-LDH compsite and the results are shown in Fig. S3 and Table S1. The N_2 adsorption-desorption isotherm is classified as the type IV with the distinct hysteresis loop in the relative pressure range of 0.6-1.0, which is a characteristic feature of mesoporous materials. The BET surface area, pore diameters and pore volume are obtained as 72.64 m^2/g, 7.43 nm and 0.13 cm^3/g, respectively.

3.2 Adsorption studies

3.2.1 Effect of contact time on CR adsorption

The effect of contact time on CR adsorption using the $NiFe_2O_4$/ZnCuCr-LDH composite was studied within 0 ~ 720 min (Fig. 3). This experiment was conducted with an initial CR concentration of 200 mg/L and an adsorbent dosage of 10g/L. The adsorption of CR is rapid and about 77 % of CR is uptake within the initial 15 minutes resulting from abundant adsorption sites of the porous composite. Then the adsorption slows down due to the most of adsorption sites are occupied with time lapse[35]. The adsorption reaches equilibrium in 240 min, indicating that a complete adsorption occurred within 240 min and a maximum removal efficiency of 89 %. Thus subsequent adsorption experiments were conducted with the contact time of 240 min.

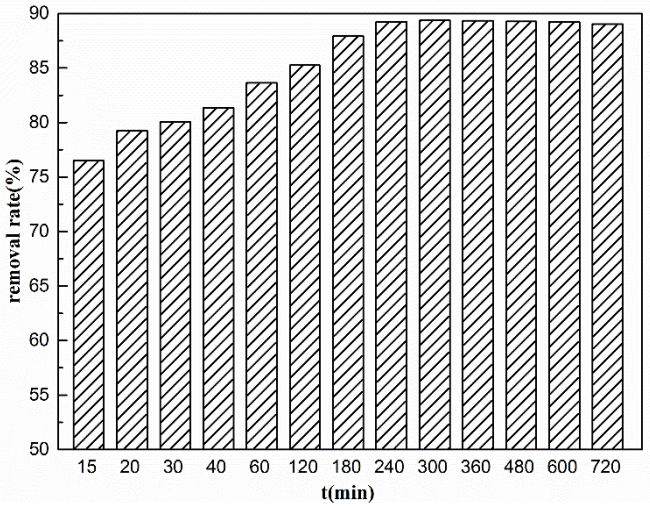

Fig. 3. Effect of contact time on CR adsorption using $NiFe_2O_4$/ZnCuCr-LDH

3.2.2 Effect of adsorbent dosage on CR adsorption

Fig.4 displays the removal rate of CR with the $NiFe_2O_4$/ZnCuCr-LDH dosage between 5 and 17.5 g/L at an initial CR concentration of 200 mg/L, and an optimal adsorbent dose of 12.5 g/L is obtained with a removal efficiency of 99%. By increasing the adsorbent dose, a higher removal rate is expected, but this is only noticed for low doses. This phenomenon could be explained by the more active sites with an increasing adsorbent dosage. However, when the addition of adsorbent reaches a very high value, e.g. 15 or 17.5 g/L, the over-added adsorbent can then not fully contact with adsorbate, a removal rate invariable is then observed[36].

Fig. 4. Effect of the adsorbent dosage on CR adsorption using $NiFe_2O_4$/ZnCuCr-LDH

3.2.3 Effect of pH on CR adsorption

In the process of adsorption, the pH is a key factor that can significantly influence not only the surface charge of the adsorbent but also the structure of dye molecules. The initial CR concentration was 200 mg/L and the adsorbent dosage was 12.5 g/L in these experiments, and the pH ranged from 2.0 to 10.0 was adjusted by 0.1 mol/L HNO_3 and NaOH. The corresponding results are presented in Fig. 5. The maximal removal efficiency of 99% is achieved at the pH of 3.0. When pH > 5, the adsorption capacity decreases due to the adsorption competition on the active sites between OH^- groups and anionic ions of CR. At a low pH, the partially dissolution of the LDH leads to a low adsorption capacity[37].

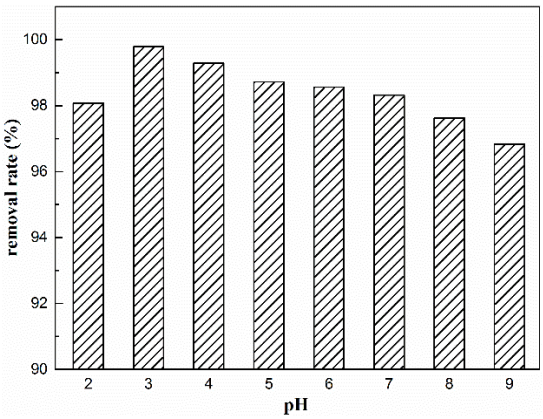

Fig. 5. Effect of pH on CR adsorption using $NiFe_2O_4$/ZnCuCr-LDH

3.2.3 Effect of initial CR concentration on CR adsorption

The experiments designed to evaluate the role of the initial CR concentration for the removal efficiency were conducted with the initial CR concentrations of 100, 150, 200, 250, 300, 350, 400, 450 and 500 mg/L, **at** the adsorbent dosage of 0.1 g/L and pH value of 3.0. Fig. 6a exhibits the effect of the initial CR concentration on CR removal. It can be seen that the removal efficiency of adsorbent is higher than 97% when the initial CR concentration rises from 100 to 450 mg/L. Fig. 6b shows that the amount of CR adsorption increases evidently with the increase of the initial CR concentration. This can be ascribed to the stronger driving force from the concentration gradient with an increased initial CR concentration to overcome the mass transfer resistance of the dye between the aqueous phase and solid phase. However, when the initial CR concentration continually increases to 500 mg/L, the removal efficiency decreased to 84 % with an also slightly smaller adsorption capacity. This can be explained by the fixed number of active sites with a specific amount of adsorbent. As the active sites are occupied, the adsorbent is insufficient to provide more active sites for CR.

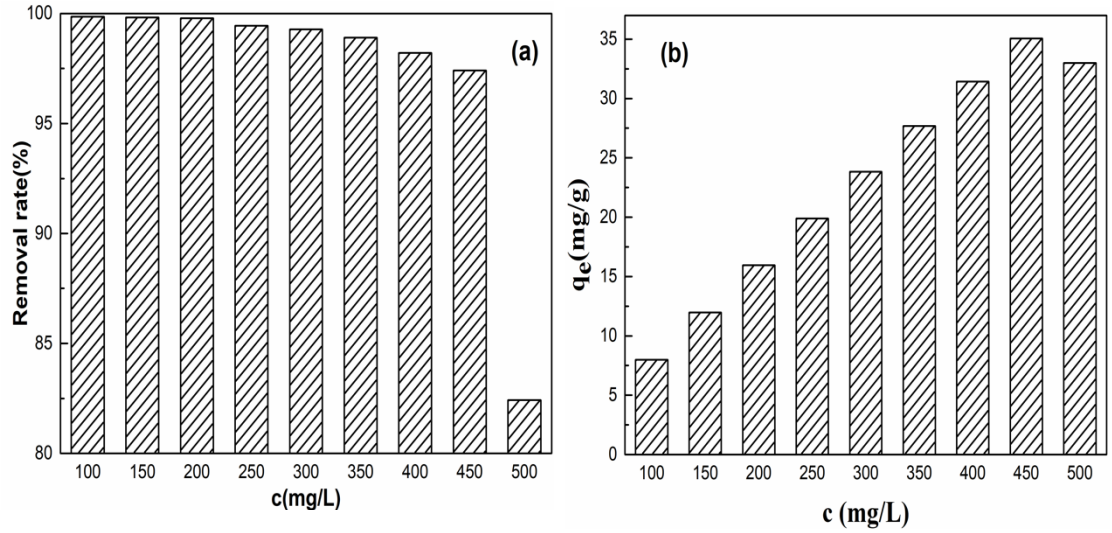

Fig. 6. Effect of the initial CR concentration on CR adsorption using $NiFe_2O_4$/ZnCuCr-LDH: (a) removal rate, (b) adsorption capacity

3.3 Adsorption kinetics

The adsorption kinetic parameters, which study the fast changing kinetic data to estimate adsorption rates and to determine possible controlling mechanism and potential rate-limiting steps, have a great practical value for technological applications. The models most widely used to study adsorption of dyes onto LDHs materials are pseudo-first-order, pseudo-second-order, Elovich and intra-particle diffusion kinetic models. The linear plots for CR adsorption onto $NiFe_2O_4$/ZnCuCr-LDH are displayed in Fig. 7 for four different models. The corresponding parameters are summarized in Table S2. Compared with the other three models, the pseudo-second-order model shows a much higher R^2 (> 0.999) and thus can be considered as the best model to describe the kinetic behavior of CR adsorption [38], indicating that the rate-controlling step involves with chemisorption or chemical bonding between the adsorbent active site and CR molecule. The slowest step determines the overall rate of the adsorption process, and this rate-limiting step can be identified by the diffusion process rather than the pseudo-second-order model. The diffusion process usually includes intra-particle diffusion, external transfer and so on. As shown in Table S2, intra-particle diffusion is more suitable to depict the diffusion behavior here. The plots of intra-particle diffusion shows multi-linearity with two stages (Fig .7c). The first stage is very steep which represents the adsorption on the external surface of $NiFe_2O_4$/ZnCuCr-LDH and is almost instantaneous. The second gentle incline indicated a comparatively slower adsorption when the adsorbate diffuses gradually into the interior surfaces of the particles and the adsorption changes to intra-particle diffusion controlled[38]. Due to the adsorption on the irregular and non-uniform sites on the steps and edges of the particles, the curves might appear multi-factor liner patterns.

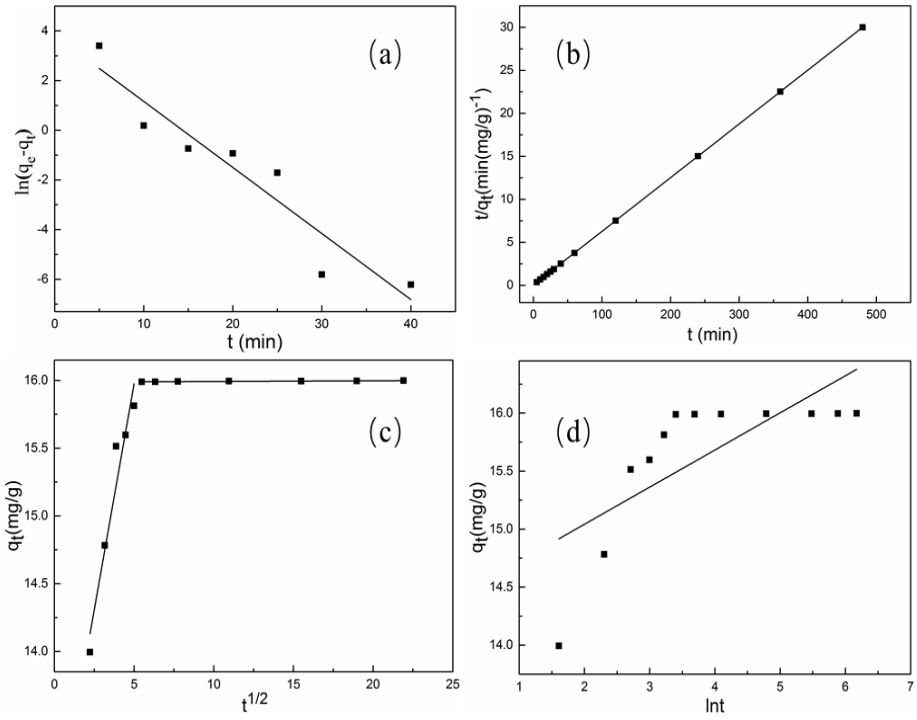

Fig 7. Kinetic models: (a) Pseudo-first-order, (b) Pseudo-second-order, (c) Intra-particle diffusion and (d) Elovich plot for adsorpyion of CR over $NiFe_2O_4$/ZnCuCr-LDH

3.4 Adsorption isotherms

Adsorption isotherm is important both to design adsorption systems and to explain adsorption mechanism, because it describes how adsorbate interact with adsorbents. The experiments were performed by varying the initial CR concentration from 200 ~ 450 mg/L and the adsorption temperature from 20 to 35 °C. Fig 8 shows the adsorption capacity increases with the temperature, which indicates the adsorption reaction of CR onto $NiFe_2O_4$/ZnCuCr-LDH is an endothermic process.

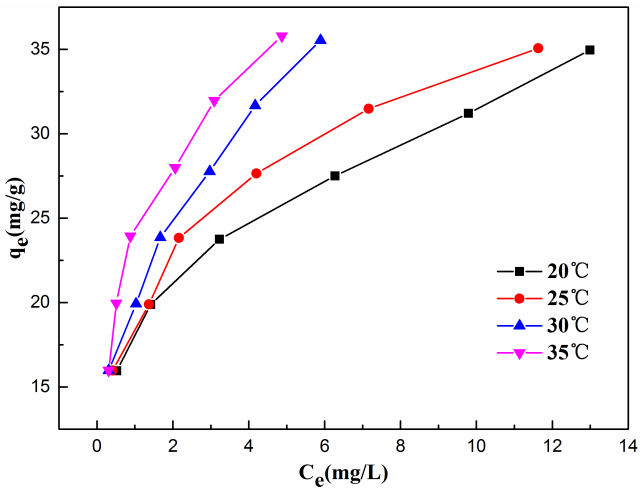

Fig 8. Adsorption isotherms of CR on $NiFe_2O_4$/ZnCuCr-LDH at different temperatures

The adsorption isotherm data were then fitted by four equilibrium models, i.e., Langmuir, Freundlich, Temkin and Dubinin-Radushkevich models: and the liner plots aere showed in Fig. 9. The fitted parameters for the four models along with regression coefficients are listed in Table S3. Table S3 show the R^2 values calculated from Langmuir isotherms are all above 0.98 and the calculated $q_{m,cal}$ (37.79 mg/g) is also very close to the experiment value (35.57 mg/g). Thus, Langmuir model is considered as the most suitable model to describe the adsorption behaviors of CR on $NiFe_2O_4$/ZnCuCr-LDH, which indicates a monolayer coverage of CR molecules on the adsorbent [39].

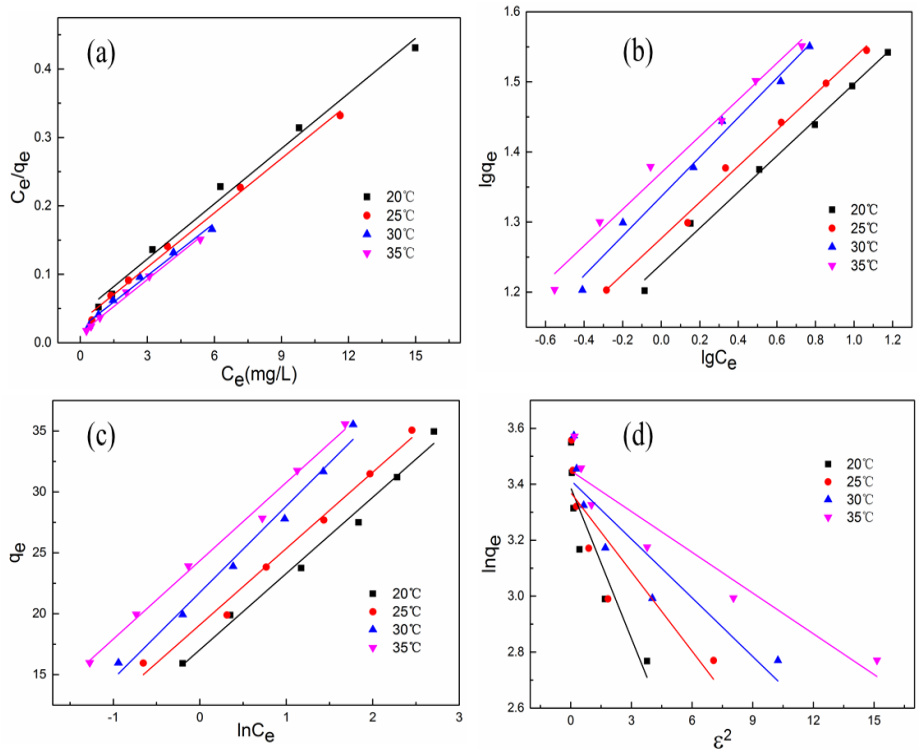

Fig 9. Plots of the Langmuir (a), Freundlich (b), Temkin (c) and D-R (d) isotherm models for the adsorption of CR on $NiFe_2O_4$/ZnCuCr-LDH

3.5 Adsorption thermodynamics

The temperature dependence of the adsorption in association with changes is provided by several thermodynamic parameters such as standard Gibbs energy (G^0), enthalpy (H^0) and entropy (S^0) of adsorption. The values of change in enthalpy ($\Delta H°$) and entropy ($\Delta S°$) were found using 1/T and ln(K) graphics, and the slope of the line is ($-\Delta H/R$), and intercept is ($\Delta S/R$), where K is the distribution cofficient ($K=q_e/C_e$), T (K) is the temperature, and R (8.314 $K \cdot mol^{-1}\ K^{-1}$) is the universal gas constant. The parameters are given in Table 2.

The negative values of ΔG^0 at different temperatures suggest the spontaneous

nature of CR adsorption on $NiFe_2O_4$/ZnCuCr-LDH. The value of ΔG^0 increases with the temperature, implying that the adsorption process is favorable at high temperature. The value of ΔH is 9.6946 KJ/mol which is much less than 40 KJ/mol, indicating the adsorption process is physical adsorption and endothermic. The positive value of ΔS^0 indicates an increase in randomness at the solid-solution interface during the adsorption process[40].

Table 2. Adsorption thermodynamic for the CR adsorption on the $NiFe_2O_4$/ZnCuCr-LDH

T(K)	ΔG^0 (kJ/mol)	$\triangle H^0$ (KJ/mol)	$\triangle S^0$ (J/mol·K)
293K	-3.8403	9.6946	46.0739
298K	-4.0650		
303K	-4.1982		
308K	-4.5584		

3.5 Adsorption mechanism

For a better understanding of of the adsorption mechanism, XRD analysis was conducted to $NiFe_2O_4$/ZnCuCr-LDH after CR removal (Fig S5). Compared with the $NiFe_2O_4$/ZnCuCr-LDH, the peak intensities of the characteristic lines for LDH in LDH-CR are weakened, implying that the adsorption of CR over LDH impacts the crystallinity of LDH which drops from 75% to 60%. Fig S6 shows that the color of the adsorbent changes from brown to black after CR adsorption, further confirming the successful adsorption of CR onto LDH.

Fig.10 demonstrates the adsorption mechanism of CR on $NiFe_2O_4$/ZnCuCr-LDH. The adsorption of CR can be described as a three- step process, involving[41]: firstly, CR is dissolved in the aqueous solution, and the sulphonate groups (A-SO_3Na) on the dye molecular are ionized to anions and cations (Eq 14); then the dye molecular anions are attracted to the surface of LDH through electrostatic forces; finally, the intercalation of NO_3^- anions is replaced by SO_3^- anions of CR via anion exchange[42].

$$A\text{-}SO_3Na \xrightarrow{H_2O} A\text{-}SO_3^- + Na^+ \quad (14)$$

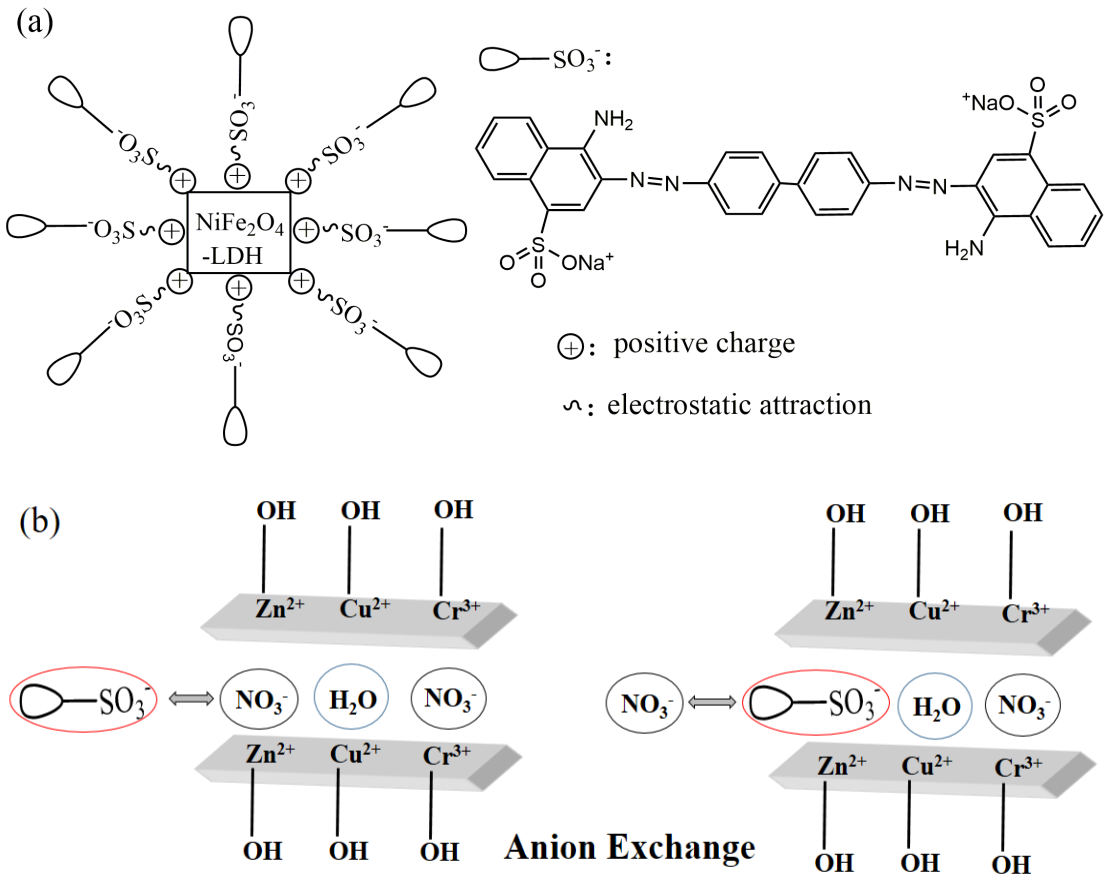

Fig.10 Schematic diagram of the adsorption mechanism of CR on $NiFe_2O_4$/ZnCuCr-LDH

4 Conclusions

In this work, we demonstrate a mesoporous magnet $NiFe_2O_4$/ZnCuCr-LDH composite prepared from saccharin wastewater by a facile hydrothermal method and its potential for practical adsorption application in wastewater treatment. During the process, about 82% COD of saccharin wastewater was removed and iron was fully re-utilized. The adsorption of CR on $NiFe_2O_4$/ZnCuCr-LDH was studied under different conditions by using single-factor experiments, which offered the optimal adsorption conditions (pH of 3 and adsorbent dose of 12.5 g/L). Under these conditions, the adsorbent exhibited a high removal efficiency more than 97% with a very wide initial CR concentration ranging from 150 ~ 450 mg/L. The adsorption kinetics study showed that the experimental data were in good agreement with pseudo-second-order kinetic model and Langmuir adsorption isotherm model with a high adsorption rate. Adsorption thermodynamic suggested that the adsorption process was endothermic and spontaneous in nature. The adsorption mechanism can be deduced that it was mainly electrostatic attraction and anion exchange. The simple synthesis and separation process, together with the excellent adsorption performance of the porous magnet composite, shows a good potential for this process to be used in practical wastewater treatment application.

References

[1] Moussavi G, Barikbin B, Mahmoudi M. The removal of high concentrations of phenol from saline wastewater using aerobic granular SBR[J]. Chemical Engineering Journal, 2010, 158(3): 498-504.

[2] Chen D, Li Q, Shao L, et al. Recovery and application of heavy metals from pickling waste liquor (PWL) and electroplating wastewater (EPW) by the combination process of ferrite nanoparticles[J]. Desalination and Water Treatment, 2016, 57(60): 29264-29273.

[3] Yue L, Wang K, Guo J, et al. Enhanced electrochemical oxidation of dye wastewater with Fe 2 O 3 supported catalyst[J]. Journal of Industrial and Engineering Chemistry, 2014, 20(2): 725-731.

[4] Rache M L, García A R, Zea H R, et al. Azo-dye orange II degradation by the heterogeneous Fenton-like process using a zeolite Y-Fe catalyst—Kinetics with a model based on the Fermi's equation[J]. Applied Catalysis B: Environmental, 2014, 146: 192-200.

[5] Cai C, Wang L, Gao H, et al. Ultrasound enhanced heterogeneous activation of peroxydisulfate by bimetallic Fe-Co/GAC catalyst for the degradation of Acid Orange 7 in water[J]. Journal of Environmental Sciences, 2014, 26(6): 1267-1273.

[6] Fu F, Wang Q. Removal of heavy metal ions from wastewaters: a review[J]. J Environ Manage, 2011, 92(3): 407-18.

[7] Sun Y, Zhou J, Cai W, et al. Hierarchically porous NiAl-LDH nanoparticles as highly efficient adsorbent for p-nitrophenol from water[J]. Applied Surface Science, 2015, 349: 897-903.

[8] Zeng Y G, Li L. Study on Treatment of Heavy Metal Lons of Chemical Wastewater by Ion Exchange Resin[J]. Advanced Materials Research, 2014, 955-959: 2230-2233.

[9] Barakat M A, Kumar R. CHAPTER 10. Modified and New Adsorbents for Removal of Heavy Metals from Wastewater[J], 2014: 193-212.

[10] Magnenet C, Jurin F E, Lakard S, et al. Polyelectrolyte modification of ultrafiltration membrane for removal of copper ions[J]. Colloids and Surfaces A: Physicochemical and Engineering Aspects, 2013, 435: 170-177.

[11] Zhang J, Chen S, Zhang Y, et al. Reduction of acute toxicity and genotoxicity of dye effluent

using Fenton-coagulation process[J]. J Hazard Mater, 2014, 274: 198-204.
[12] Rajamanickam D, Shanthi M. Photocatalytic degradation of an azo dye Sunset Yellow under UV-A light using TiO2/CAC composite catalysts[J]. Spectrochim Acta A Mol Biomol Spectrosc, 2014, 128: 100-8.
[13] Xu P, Han H, Zhuang H, et al. Advanced treatment of biologically pretreated coal gasification wastewater by a novel integration of heterogeneous Fenton oxidation and biological process[J]. Bioresour Technol, 2015, 182: 389-92.
[14] Yu L, Luo Y-M. The adsorption mechanism of anionic and cationic dyes by Jerusalem artichoke stalk-based mesoporous activated carbon[J]. Journal of Environmental Chemical Engineering, 2014, 2(1): 220-229.
[15] Ji M, Su X, Zhao Y, et al. Effective adsorption of Cr(VI) on mesoporous Fe-functionalized Akadama clay: Optimization, selectivity, and mechanism[J]. Applied Surface Science, 2015, 344: 128-136.
[16] Chen H, Yan T, Jiang F. Adsorption of Cr(VI) from aqueous solution on mesoporous carbon nitride[J]. Journal of the Taiwan Institute of Chemical Engineers, 2014, 45(4): 1842-1849.
[17] Xiao Q, Sun Y, Zhang J, et al. Size-dependent of chromium (VI) adsorption on nano α-Fe2O3 surface[J]. Applied Surface Science, 2015, 356: 18-23.
[18] Mohapatra M, Anand S. Synthesis and applications of nano-structured iron oxides/hydroxides – a review[J]. International Journal of Engineering Science & Technology, 2010, 2: 127-146.
[19] Chen D, Mei C Y, Yao L H, et al. Flash fixation of heavy metals from two industrial wastes into ferrite by microwave hydrothermal co-treatment[J]. J Hazard Mater, 2011, 192(3): 1675-82.
[20] Sen R, Jain P, Patidar R, et al. Synthesis and Characterization of Nickel Ferrite (NiFe2O4) Nanoparticles Prepared by Sol- Gel Method[J]. Materials Today: Proceedings, 2015, 2(4-5): 3750-3757.
[21] Joshi S, Kumar M, Chhoker S, et al. Structural, magnetic, dielectric and optical properties of nickel ferrite nanoparticles synthesized by co-precipitation method[J]. Journal of Molecular Structure, 2014, 1076: 55-62.
[22] Nawale A B, Kanhe N S, Patil K R, et al. Magnetic properties of thermal plasma synthesized nanocrystalline nickel ferrite (NiFe2O4)[J]. Journal of Alloys and Compounds, 2011, 509(12): 4404-4413.
[23] Wang J, Ren F, Yi R, et al. Solvothermal synthesis and magnetic properties of size-controlled nickel ferrite nanoparticles[J]. Journal of Alloys and Compounds, 2009, 479(1-2): 791-796.
[24] Zou B F, Liu Y F, Wang Y Q. Facile synthesis of highly water-dispersible and monodispersed Fe3O4 hollow microspheres and their application in water treatment[J]. Rsc Advances, 2013, 3(45): 23327-23334.
[25] Rameshbabu R, Ramesh R, Kanagesan S, et al. Synthesis of superparamagnetic ZnFe2O4 nanoparticle by surfactant assisted hydrothermal method[J]. Journal of Materials Science: Materials in Electronics, 2013, 24(11): 4279-4283.
[26] Peligro F R, Pavlovic I, Rojas R, et al. Removal of heavy metals from simulated wastewater by in situ formation of layered double hydroxides[J]. Chemical Engineering Journal, 2016, 306: 1035-1040.
[27] Yang Z, Wang F, Zhang C, et al. Utilization of LDH-based materials as potential adsorbents and photocatalysts for the decontamination of dyes wastewater: a review[J]. RSC Adv., 2016, 6(83):

79415-79436.
[28] Theiss F L, Ayoko G A, Frost R L. Synthesis of layered double hydroxides containing Mg2+, Zn2+, Ca2+ and Al3+ layer cations by co-precipitation methods—A review[J]. Applied Surface Science, 2016, 383: 200-213.
[29] Lei C S, Zhu X F, Zhu B C, et al. Superb adsorption capacity of hierarchical calcined Ni/Mg/Al layered double hydroxides for Congo red and Cr(VI) ions[J]. Journal of Hazardous Materials, 2017, 321: 801-811.
[30] Chen D, Li Y, Zhang J, et al. Magnetic Fe3O4/ZnCr-layered double hydroxide composite with enhanced adsorption and photocatalytic activity[J]. Chemical Engineering Journal, 2012, 185-186: 120-126.
[31] De Sá F P, Cunha B N, Nunes L M. Effect of pH on the adsorption of Sunset Yellow FCF food dye into a layered double hydroxide (CaAI-LDH-NO3)[J]. Chemical Engineering Journal, 2013, 215-216: 122-127.
[32] Zhang G, Lin B, Qiu Y, et al. Highly efficient visible-light-driven photocatalytic hydrogen generation by immobilizing CdSe nanocrystals on ZnCr-layered double hydroxide nanosheets[J]. International Journal of Hydrogen Energy, 2015, 40(14): 4758-4765.
[33] Sahoo P, Shrestha R G, Shrestha L K, et al. Surface Oxidized Carbon Nanotubes Uniformly Coated with Nickel Ferrite Nanoparticles[J]. Journal of Inorganic and Organometallic Polymers and Materials, 2016, 26(6): 1301-1308.
[34] Wang C, Ma B, Xu S, et al. Visible-light-driven overall water splitting with a largely-enhanced efficiency over a Cu2O@ZnCr-layered double hydroxide photocatalyst[J]. Nano Energy, 2017, 32: 463-469.
[35] Deng L, Shi Z, Peng X, et al. Magnetic calcinated cobalt ferrite/magnesium aluminum hydrotalcite composite for enhanced adsorption of methyl orange[J]. Journal of Alloys and Compounds, 2016, 688: 101-112.
[36] Garg V K, Gupta R, Bala Yadav A, et al. Dye removal from aqueous solution by adsorption on treated sawdust[J]. Bioresource Technology, 2003, 89(2): 121-124.
[37] Ahmed I M, Gasser M S. Adsorption study of anionic reactive dye from aqueous solution to Mg–Fe–CO3 layered double hydroxide (LDH)[J]. Applied Surface Science, 2012, 259: 650-656.
[38] Bhattacharyya K G, Sharma A. Adsorption of Pb(II) from aqueous solution by Azadirachta indica (Neem) leaf powder[J]. J Hazard Mater, 2004, 113(1-3): 97-109.
[39] Wu F C, Tseng R L, Juang R S. Comparative adsorption of metal and dye on flake- and bead-types of chitosans prepared from fishery wastes[J]. Journal of Hazardous Materials, 2000, 73(1): 63-75.
[40] Gök A, Gök M K, Aşçı Y S, et al. Equilibrium, kinetics and thermodynamic studies for separation of malic acid on layered double hydroxide (LDH)[J]. Fluid Phase Equilibria, 2014, 372: 15-20.
[41] Lu L, Li J, Ng D H L, et al. Synthesis of novel hierarchically porous Fe3O4@MgAl–LDH magnetic microspheres and its superb adsorption properties of dye from water[J]. Journal of Industrial and Engineering Chemistry, 2017, 46: 315-323.
[42] Yang K, Yan L-G, Yang Y-M, et al. Adsorptive removal of phosphate by Mg–Al and Zn–Al layered double hydroxides: Kinetics, isotherms and mechanisms[J]. Separation and Purification Technology, 2014, 124: 36-42.

Supporting information

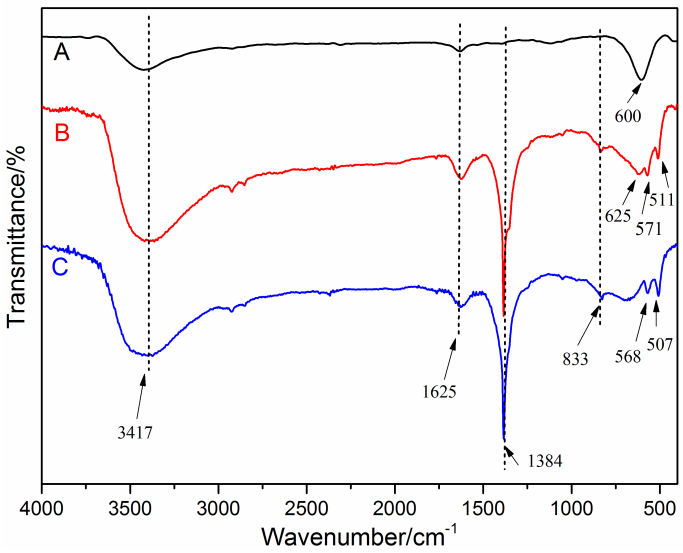

Fig.S1. IR spectra of (A) $NiFe_2O_4$, (B) $NiFe_2O_4$/ZnCuCr-LDH, (C) ZnCuCr-LDH

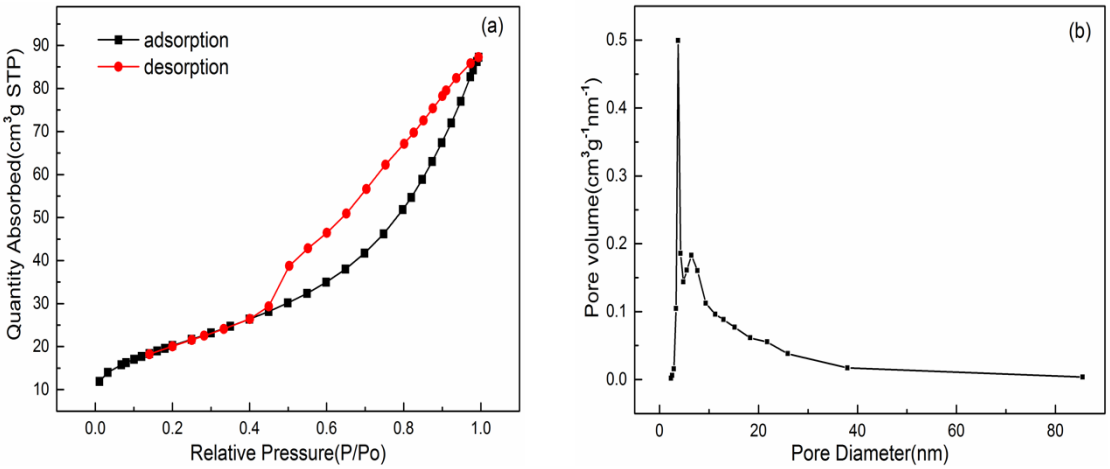

Fig.S2. (a) N_2 absorption-desorption isotherm for $NiFe_2O_4$/ZnCuCr-LDH, (b) The pore size distribution curve for the $NiFe_2O_4$/ZnCuCr-LDH.

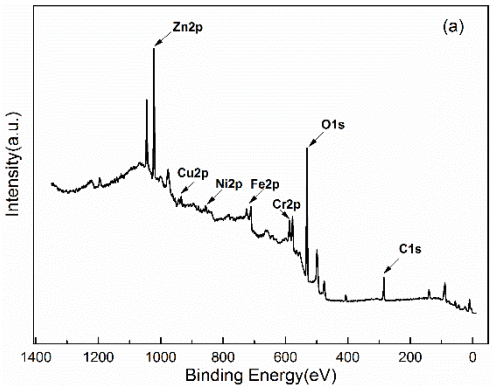

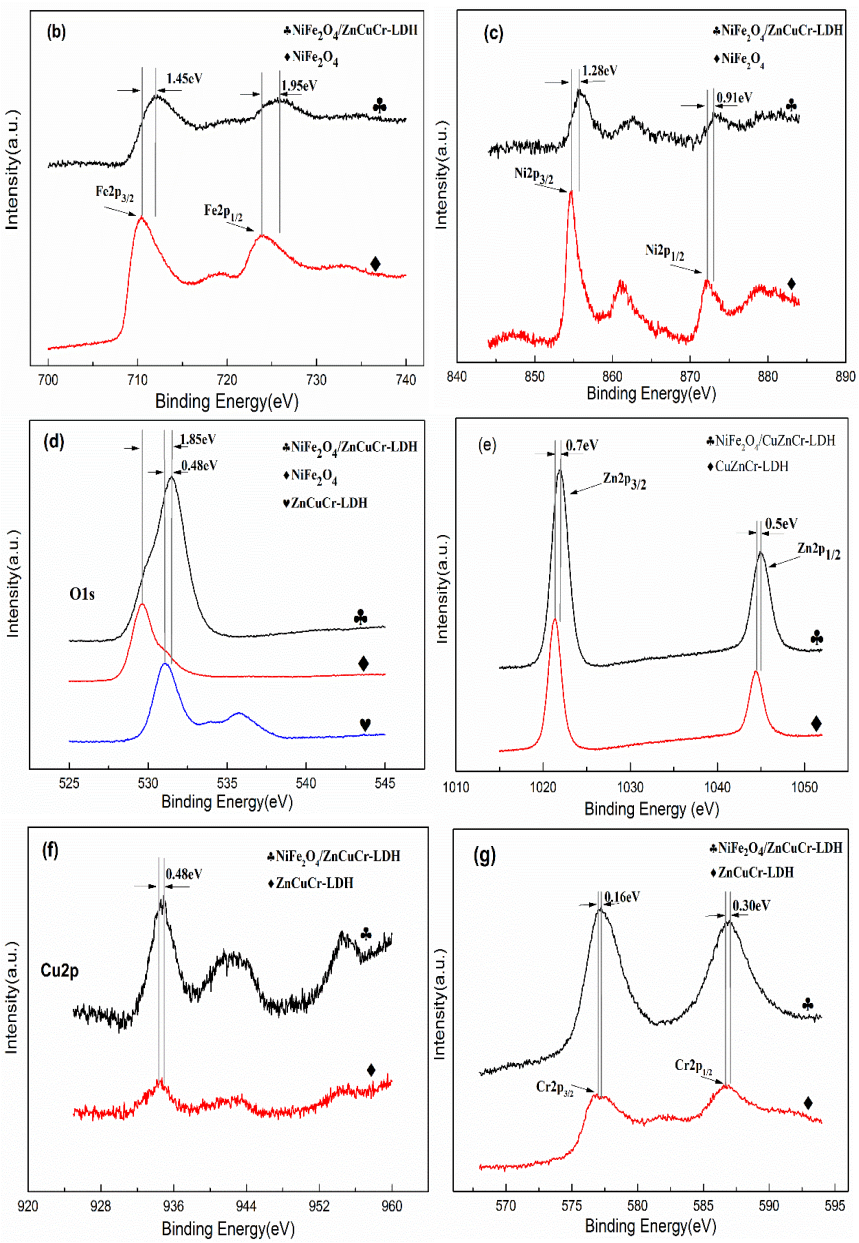

Fig. S3. (a) Survey XPS spectra of the $NiFe_2O_4$/ZnCuCr-LDH composite, (b) Fe 2p XPS spectra, (c) Ni 2p XPS spectra, (d) O1s XPS spectra, (e) Zn 2p XPS spectra, (f) Cu 2p XPS spectra and (g) Cr 2p XPS spectra.

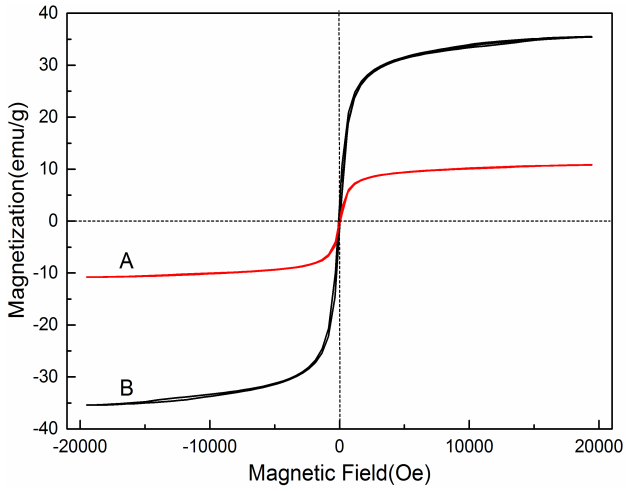

Fig. S4. Magnetization curves of $NiFe_2O_4$/ZnCuCr-LDH(A) and pure $NiFe_2O_4$(B) (inset: separation of the $NiFe_2O_4$/ZnCuCr-LDH from the treated CR solution using an external magnetic field)

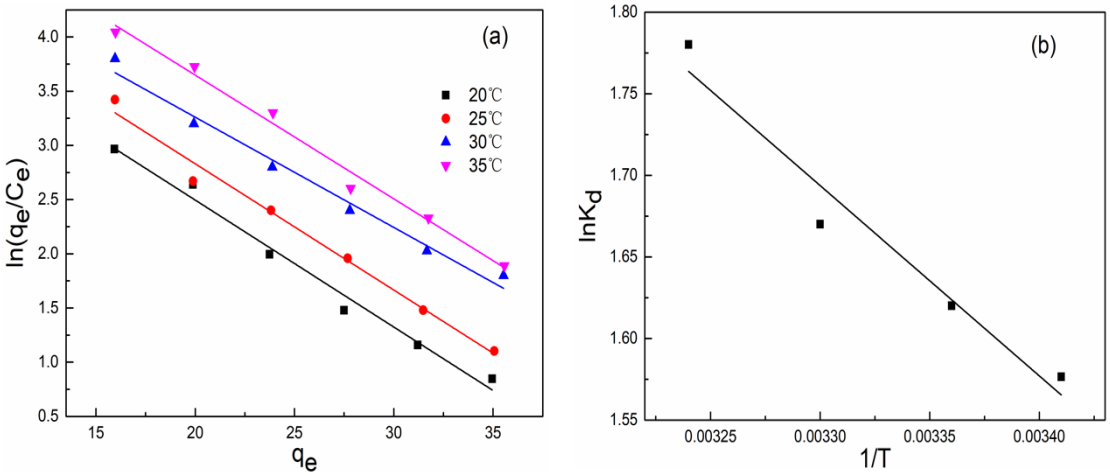

Fig. S5. (a) Plots of ln (q_e/C_e) as a function of for the CR adsorption on the $NiFe_2O_4$/ZnCuCr-LDH. (b) Van't Hoff plot for the CR adsorption on the $NiFe_2O_4$/ZnCuCr-LDH

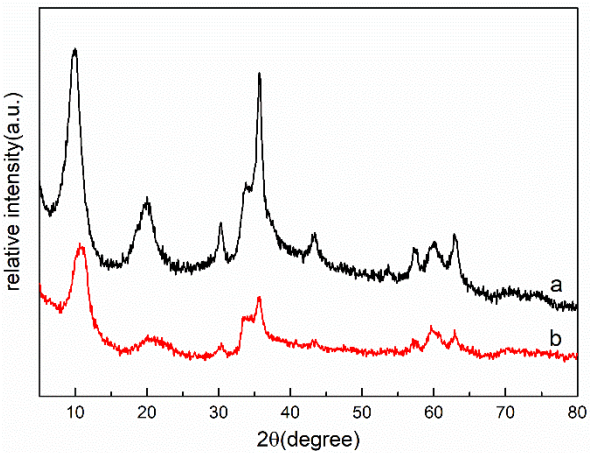

Fig. S6 XRD patterns of (a) ZnCuCr-LDH, (b) $NiFe_2O_4$/ZnCuCr-LDH

Fig. S7 Picture of $NiFe_2O_4$/ZnCuCr-LDH (NLDH) before and after CR removal

Table S1 BET surface area, pore volume, and pore diameter of different samples

Samples	BET surface area (m^2/g)	pore volume (cm^3/g)	Pore diameter (nm)
$NiFe_2O_4$/ZnCuCr-LDH	72.64	0.13	7.43

Table S2. Pseudo-first-order, pseudo-second-order, Intra-particle diffusion and Elovich kinetic parameters for CR adsorption on $NiFe_2O_4$/ZnCuCr-LDH

Kinetic models	**Pseudo-first-order**		**Pseudo-second-order**		**Intra-particle diffusion**		**Elovich**	
	k_1 (min^{-1})	R^2	k_2 ($g \cdot mg^1 \cdot min^{-1}$)	R^2	k_i ($mg \cdot g^1 \cdot min^{-0.5}$)	R^2	A	R^2
	0.2659	0.8816	0.0624	1.0000	0.6675	0.9216	0.3199	0.4987
					4.8671×10^{-4}	0.9233		

Table S3. Adsorption isotherm parameters of Langmuir, Freundlich, Temkin and D-R models for the adsorption of CR on $NiFe_2O_4$/ZnCuCr-LDH

Model		T(℃)			
		20	25	30	35
Langmuir	$K_L(L \cdot mg^{-1})$	0.6423	0.8560	1.2115	1.9444
	$q_{max}(mg \cdot g^{-1})$	37.2301	37.7929	39.0625	38.0952
	R^2	0.9902	0.9944	0.9875	0.9931
Freundlich	$K_F(mg^{1-1/n} \cdot L^{1/n} \cdot g^{-1})$	17.3724	18.9095	21.6970	23.4596
	n	3.8852	3.8797	3.5491	3.8407

	R^2	0.9897	0.9933	0.9827	0.9796
Temkin	A_T(L·mg^{-1})	15.2219	21.0537	21.4962	44.1751
	B_T(kJ·mol^{-1})	0.3893	0.3956	0.3554	0.3985
	R^2	0.9858	0.9863	0.9829	0.9913
D-R	q_{max}(mg·g^{-1})	29.5966	29.0977	30.4437	31.4453
	β(mol^2·kJ^{-2})	0.1797	0.0945	0.0699	0.0486
	R^2	0.8028	0.6966	0.7916	0.8893